Target Motion Tracking in MRI-guided Transrectal Robotic Prostate Biopsy

Hadi Tadayyon, *Member, IEEE,* Andras Lasso, *Member, IEEE,* Aradhana Kaushal, Peter Guion, *Member, IEEE,* and Gabor Fichtinger, *Member, IEEE*

***Abstract*—Purpose: MRI-guided prostate needle biopsy requires compensation for organ motion between target planning and needle placement. Two questions are studied and answered in this work: (1) is rigid registration sufficient in tracking the targets with an error smaller than the clinically significant size of prostate cancer and (2) what is the effect of the number of intra-operative slices on registration accuracy and speed? Methods: We propose multislice-to-volume registration algorithms for tracking the biopsy targets within the prostate. Three orthogonal plus additional transverse intra-operative slices are acquired in the approximate center of the prostate and registered with a high-resolution target planning volume. Both rigid and deformable scenarios were implemented. Both simulated and clinical MRI-guided robotic prostate biopsy data were used to assess tracking accuracy. Results: Average registration errors in clinical patient data were 2.6 mm for the rigid algorithm and 2.1 mm for the deformable algorithm. Conclusion: Rigid tracking appears to be promising. Three tracking slices yields significantly high registration speed with an affordable error.**

***Index Terms* –registration, motion tracking and compensation, MRI, prostate cancer, biopsy**

1. INTRODUCTION

THIS paper reports the development of rigid and deformable image registration algorithms for providing intra-operative motion compensation in MRI-guided prostatic needle placement procedures. We propose to position the patient such that his prostate lies in the scanner's isocenter and acquire multiple statically set slices in this position. It is posited that full six degree-of-freedom (DOF) motion of the prostate can be recovered through the registration of a target planning MR volume and multiple MR slices acquired immediately before and after needle insertion. Orthogonal tracking slices are acquired with ordinary anatomical imaging sequences through the scanner's console.

Prostate cancer continues to be a worldwide health problem and the most common type of cancer among men. An estimated 217,730 new cases of prostate cancer are expected in the United States in the year 2010 [1]. A definitive diagnosis for prostate cancer requires histopathological examination of tissue samples from the patient's prostate gland. The samples are acquired through prostate biopsy, which is a minimally invasive procedure in which tissue samples are typically obtained by needle placement through the rectum (transrectal procedure) or perineum (transperineal procedure) under image guidance.

In the pursuit of more accurate biopsy, Krieger *et al.* developed transrectal robotic assistance under MR image guidance [2]. To date, their system has been used at the U.S. National Cancer Institute in a clinical trial. A diagnostic quality MR volume of the patient's pelvis was acquired before the biopsy session, which the physician studied to determine the biopsy target locations. In the biopsy session, a set of lower resolution MR slices were acquired immediately before each needle insertion to confirm biopsy locations. After proper needle adjustments were made, the needle was inserted and the core was extracted. Physicians have encountered a major dilemma in this procedure: the needle puncture marks in the prostate in the post-needle insertion image often do not match with the originally planned biopsy positions defined in the target planning volume. This is due to prostate motion and deformation between pre-needle and post-needle insertion. Patient motion occurs mostly at point of needle placement due to discomfort, which causes the prostate to press against the probe, causing it to be displaced and deformed. This clinical observation has been quantified by Xu *et al.* [3] in a recent longitudinal study of MRI-guided transrectal prostate biopsy cases accrued over several years. An average biopsy target displacement of 5.4 mm was found. Inaccurate biopsies, which are realized post-intervention, may lead to repeat biopsies. Repeat biopsies incur extra costs to the health care provider and increased health complications to the patient. This underscores the need for a system to track the prostate position throughout the biopsy procedure.

1.1 Previous Works in Prostate Image Registration

Image-based anatomical tracking is a vast topic which has attracted a large body of research. The brief review herein covers a few selected works in 3D-3D and 2D-3D (slice-to-volume) registration using non-MRI modalities and compares them to the methods that use MRI. MRI-based anatomical registration methods are also reviewed.

H. Tadayyon is currently with the Department of Medical Biophysics of the University of Toronto, Toronto, Canada. During this research he was with the Department of Electrical and Computer Engineering, Queen's University, Kingston, Canada; email: hadi.tadayyon@utoronto.ca

A. Lasso is with the School of Computing, Queen's University, Kingston, Canada

P. Guion and A. Kaushal are with National Institutes of Health, Bethesda, USA

G. Fichtinger (the corresponding author) is with the School of Computing, Queen's University, Kingston, Canada; email: gabor@cs.queensu.ca

In the framework of ultrasound (US), volume-to-volume registration methods [4] and slice-to-volume registration methods [5] have been proposed for transrectal ultrasound (TRUS)-guided prostate biopsy target tracking. However, with US only systematic sampling is possible (with predefined target locations), because typically, sub-structures or lesions within the prostate are not visible in US images [6]. For improved prostate margin and lesion visualization, fusion of interventional US with pre-operative MRI has been suggested for prostate biopsy [7. 8]. This method was reported to increase the yield of prostate biopsies as opposed to conventional TRUS for patients with previously negative biopsies [7]. Methods of multi-protocol MRI to histology registration of the prostate have also been developed in an effort to obtain an accurate estimate of the spatial extent of prostate cancer and define quantitative disease signatures of the prostate in an MR image [9].

The feasibility of using MRI as an alternative tool for surgical navigation in prostate biopsy was studied by Hata *et al.* [10]. Through patient trials they proved that T2-weighted interventional MR imaging with 3D visualization software can be used to guide needle placement in prostate biopsies. For MRI-guided target tracking, radio-frequency (RF) signal based and image based methods have been proposed. In RF signal based tracking, the subject is scanned using a custom designed imaging sequence before and after motion. Translational motion information is then computationally derived from the resulting echo of the RF coil. Hata *et al*. [11] developed an intra-operative MRI registration algorithm using projection profile matching of the RF echo. The algorithm was reported to be fast and semi-real time. The drawbacks of this technique are twofold: lack of 3D positional information and the requirement to access the MRI machine's control sequence, which is not widely available for average care facilities and cannot be considered as clinically practical. For interventional applications that require 3D visual information of a moving subject, 3D registration algorithms have been introduced. Of particular interest in the past decade has been the evaluation of 3D non-rigid registration techniques for MRI-guided brachytherapy procedures, including finite element [12] and B-spline methods [13]. However, limited effort has been made in the improvement of temporal performance of MRI-based registration algorithms in general.

A clinically practical solution to the prohibitively long volume acquisition and registration times and unavailability of custom scanning sequences is multislice-to-volume registration. This technique wraps around the idea of aligning intra-operative slice images to the pre-operative volume image to recover subject motion. Intra-operative volume acquisition time is saved by using a pre-operative reference volume acquired prior to the intervention and pre-calibrating the surgical tool(s) to this volume. In the case of transrectal prostate biopsies, the surgical tool is the needle placement system (Fig. **1**). Multiple statically set slices are acquired at the scanner's isocenter, which eliminate the need for a custom MR scanning sequence. For consistency with the context of tracking, intra-operative slices/volume will be referred to as tracking slices/volume and the preoperative volume will be referred to as the reference volume.

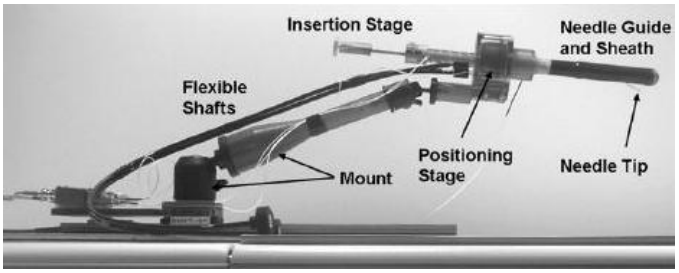

Fig. 1: Side view of the MRI-compatible intra-prostatic needle placement device developed by Krieger *et al.* [2]

In the context of multislice-to-volume registration, two works in particular inspired our project: Fei *et al.* [14] and Gill *et al*. [15]. Fei *et al.* developed a multislice-to-volume registration algorithm with application to radio-frequency thermal ablation of prostate cancer, in which 15 actual intra-operative prostate MRI slices from transverse, sagittal, and coronal orientations were registered to a pre-operative MR volume, respectively. The slices from each orientation were independently registered to the pre-operative volume, meaning that three independent registrations were performed and the results were compared. Their algorithm featured a multi-resolution approach with an automatic restart. The automatic restart applied a random perturbation to the last transformation parameters found by the registration in order to escape from potential local minimum of the cost function and re-execute the registration process.

Gill *et al.* addressed the problem of local extreme traps and the inefficiency of Fei's optimization. They eliminated the need for restarting the registration by performing a multi-resolution registration alone on a volume of interest (VOI), and incorporated transverse and sagittal simulated slices centered at the prostate. Previously [16], we developed rigid and deformable tracking algorithms which were tested on clinical data. This paper is built upon [16] with the addition of registration parameter analysis, in which simulated rigid and deformable registration tests were performed on varying number of slices, mutual information sample size, B-spline grid resolution, and slice thickness.

1.2 Objectives

The objective of this paper is defined in two parts: (1) to develop rigid and deformable multislice-to-volume registration techniques to account for and accurately quantify prostate motion in MRI-guided transrectal biopsy procedure. (2) to determine the effect of the number of tracking slices on the registration accuracy and time.

Six degree-of-freedom motion (translations along and rotations about x, y and z axes) as well as deformable displacement field must be recovered. In the scope of prostatic needle placement, a registration error less than 3 mm is considered to be sufficiently accurate as it is comparable to the diameter of a standard biopsy needle and smaller than the

radius of the clinically significant tumor which is about 4 mm [17]. The objective of tracking is to ascertain current prostate position prior to insertion of the biopsy needle. Tracking is requested by the physician and executed by the operator through the console, so the requirement for speed is timely response to the physician's requests. Based on our experience in multiple clinical trials with the device of Krieger *et al.* the preferred processing time is 1 minute.

1.3 Contributions

Our present contributions are threefold: (1) Development of deformable prostate tracking scheme using pre-operative volume MRI and intra-operative slice MRI. To our knowledge, this approach with aforementioned specifications has not been attempted by other groups, though volume-to-volume approaches have been proposed [18]. (2) Elimination of the need for random restarts and multi-resolution registration in the rigid scheme that hampered earlier works [14, 15]. As previously mentioned, random restarts and multi-resolution registration reduce temporal performance. We found that decoupled optimization improved temporal performance as opposed to random restarts and multi-resolution approaches. Decoupled optimization is a technique whereby translations are first optimized and then the results are used as initial center of rotation to optimize rotations.
(3) Analysis of the performance on simulated intra-operative and clinical MRI-guided prostate biopsy data.

2. MEHOTDS

Our tracking algorithm was validated on two types of data, simulated patient and real patient data. Detailed explanation of these data groups will be covered in sections 2.6 and 2.7. Motion-simulated slices were generated from a reference volume by rigid translation and rotation, and a deformation defined by an FEM model of the prostate. The motion-simulated volume was registered back to the reference volume to recover the ground truth motion. Real patient data involved registration of pre-needle insertion slices to the target planning volume. Rigid and deformable registration tests were performed on both data groups and analyzed separately.

2.1 Metric

In motion tracking applications where a low-resolution MRI is registered to high-resolution MRI, cross-correlation (CC) and mutual information (MI) are commonly used as the similarity metrics in a multi-resolution approach [14, 15] Intensity scaling caused by MR coil response inhomogeneity does not affect MI, which makes it a suitable metric for MRI registration problems [14], hence, our choice of metric.

2.2 Preprocessing

The input image formatting pipelines for the aforementioned data types are illustrated in Fig. **2** and Fig. **3**. The pre-processing stage of our algorithm must place the slices in the correct position and orientation in a sparse volume. The slice origin and direction cosines read from the DICOM tags are used to resample the slices into a sparse volume. The bounding box of the prostate is defined as the volume of interest in the sparse volume. To form the simulated data, initial random deformation field followed by rigid perturbation were computationally applied to the reference volume, as shown in Fig. **2**. Detailed explanation of how the deformation field and rigid perturbations were created is provided in section 2.6.

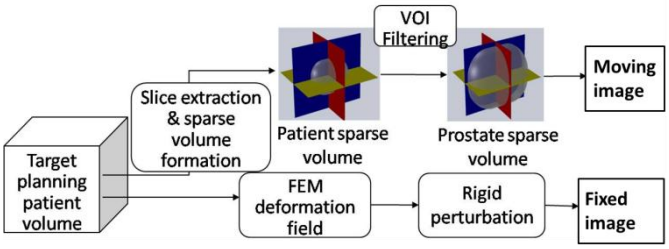

Fig. 2: The image preprocessing pipeline for simulation data

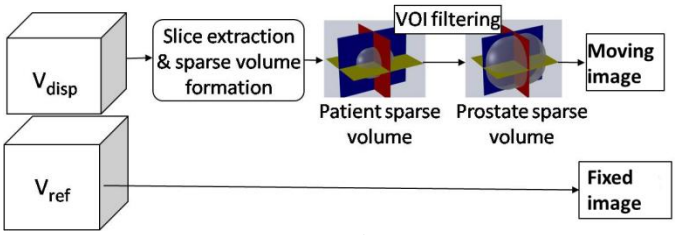

Fig. 3: The image preprocessing pipeline for clinical pair data

2.3 Filtering and Volume of Interest

To constrain the registration to the prostate region, A VOI was defined as a bounding box enclosing the reference volume prostate, which was defined by an origin and x, y, z extents. Since the precise location of the tracking volume prostate is unknown, the same VOI was defined for the tracking volume, which provided a reasonable initial estimate of the location. The rigid registration scheme assumes that the VOI undergoes rigid motion from one frame to another, meaning that the prostate is assumed to be rigid. The deformable registration scheme used the same VOI, but does not assume rigidity.

Once the VOI was defined, two spatial filters were applied to the VOI to enhance the prostate image. A histogram matching filter was first applied to the moving image to match the intensities of the fixed image. The moving and fixed images were then passed through a Gaussian smoothing filter in order to obtain smooth intensity estimates for the mutual information similarity metric. Random intensity samples were drawn from the fixed image to calculate the joint probability distribution function. The optimal sample size was determined through a series of tests (section 3.1)

2.4 Initialization and Registration

The tracking volume was initially positioned such that its geometric center coincided with the geometric center of the reference volume. This was an appropriate initialization because for every scan the patient was positioned such that his prostate lied in the scanner's isocenter.

The algorithmic concept behind registration is to find the optimum transformation matrix which best aligns the target image to the source image so as to obtain maximum overlap of a certain structure of interest. In our case, the structure of interest is the prostate. This method is referred to as intensity-based because the cost function to be optimized is a similarity metric, which attempts to find the highest match of intensities of the input images. The metric used in our case is MI. Fig. **4** shows the flow of the registration algorithm. The registration is performed in two stages: A rigid registration is first performed to obtain an initial pose of the pre-needle volume, which is then non-rigidly registered to the fixed, rigid reference volume. In the diagram, I(i,j,k) represents an image, defined by a 3D matrix of intensities whose voxel locations are specified by image coordinates i, j and k.

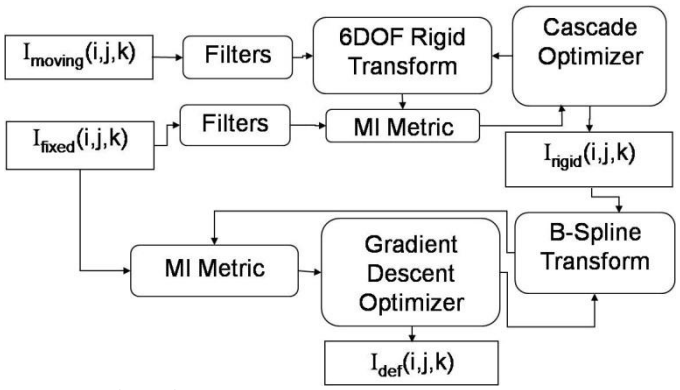

Fig. 4: Workflow of the registration algorithm

Two metrics were defined which measures the accuracy of our registration: surface distance error (SDE) and target registration error (TRE). SDE was defined as the mean surface distance error between the segmented prostate surfaces of the reference volume and the motion-simulated volume after registration.

The SDE for the simulated registrations was computed by selecting the vector elements of the error field that lie on the surface of the prostate and averaging them over the prostate surface, mathematically expressed as,

$$SDE_{sim} = \frac{\sum_{s=0}^{N_s} \left| \boldsymbol{E}\left(\boldsymbol{x}(s), \boldsymbol{y}(s), \boldsymbol{z}(s)\right) \right|}{N_s} \quad (1)$$

where $[\boldsymbol{x}(s), \boldsymbol{y}(s), \boldsymbol{z}(s)]$ represents an array consisting of all the points on the segmented prostate surface (Ns = 4716 points), **E** is the error field matrix, and || represents vector length. Hence, SDE is the average of the error field evaluated over the prostate surface. To validate the clinical data registrations, we manually segmented the prostates in the reference and tracking volumes and computed the mean SDE before and after registration. The points making up the prostate surfaces, denoted as P_{fixed} and P_{moving}, were formatted in a $N_s \times D$ array, where N_s is the number of points in the surface (4716) and D is the image dimension (3). The moving surface points were then re-sorted according to a nearest neighbor search [19] algorithm such that the distance between corresponding fixed and moving points was minimized. Equation 2 mathematically expresses the formulation of SDE for actual patient data.

$$SDE_{pat} = \frac{\sum_{i=0}^{N_s} |P_{fixed}(i) - P_{moving}(i)|}{N_s} \quad (2)$$

TRE was defined as the mean distance between the ground truth and registered positions of biopsy points,

$$TRE = \frac{\sum_{\tau=0}^{N_\tau} \left| \boldsymbol{E}\left(\boldsymbol{x}(\tau), \boldsymbol{y}(\tau), \boldsymbol{z}(\tau)\right) \right|}{N_\tau} \quad (3)$$

where $[\boldsymbol{x}(\tau), \boldsymbol{y}(\tau), \boldsymbol{z}(\tau)]$ is the biopsy target position vector consisting of six targets and N_τ is the number of biopsy targets. TRE is a subset of SDE since the error vectors at the six biopsy positions are sampled from the error field and averaged to obtain this metric. The six biopsy positions were defined according to the sextant biopsy method, in which three cores were extracted from the peripheral zone of the base, mid, and apex of the right part, and three mirrored cores on the left part of the prostate.

2.5 Transformations and Optimizations

Rigid transformation optimization proceeds in a cascade model, in which the translation parameters are optimized using the CMA Evolutionary Strategy (CMA-ES) [20]. Following translation, rotation is optimized by gradient descent optimization. For our application, the CMA-ES was not able to optimize a 6-DOF search space as it diverged on rotations regardless of scaling. Thus, we decoupled the translation and rotation optimizations and used the CMA-ES for the parameters that varied the most, i.e. the translation. The gradient descent optimizer converges quickly and accurately for parameters that have a smaller variation range, i.e. the rotations in our case. The order of optimization is key here; translation must be optimized first in order to align the center of rotation of the moving image with the geometric center of the fixed image. In cases where the prostate's center of mass is not aligned in the images, optimizing for rotation first results in further divergence from the solution.

We feed the rigidly registered pre-needle volume to a deformable registration algorithm, which runs through a two-level registration pyramid using coarse B-spline grid (40 x 40 x 20 mm resolution) followed by a finer grid (13 x 13 x 6.7 mm resolution), where the nodes of the grid act as control points. The reason for the choice of these grid sizes are explained in section 3.1. Using a gradient descent optimizer, we search the parameter space of the B-spline grid for the parameters that maximize the MI value.

2.6 Simulation Data

In order to explore the robustness, capture range and temporal performance of our tracking algorithm on pre-recorded clinical data, we created simulated tracking volumes using finite element (FE) modeling and rigid 6-degree-of-freedom perturbation to generate deformations and rigid body

motions, respectively. Using a finite element analysis software application developed by Lasso *et al.* [21], we generated 20 simulated patient MR images containing the deformed prostate due to patient motion. The FE model of the prostate/probe system is shown in Fig. **5**. Material properties of the body (spherical mesh) and the prostate were adapted from [22]; both objects were modeled as linear elastic materials, the prostate with Poisson ratio $\upsilon = 0.4$ and Young's modulus E = 21 kPa, body with $\upsilon = 0.4$ and E = 15 kPa. Patient motion causes considerable local pressure on the prostate by the transrectal probe. This pressure was modeled by prescribing force loads (of random perturbations in direction and magnitude) on the mid-posterior surface of the prostate. The FE solver was run on 20 cases involving different force loads and probe positions (1D translation normal to the rectal axis) and a ground truth deformation field was computed. Probe translation was randomized in the range of (-2 mm < Tx < 2 mm). The coordinate system was defined such that the rectal axis was aligned with the z axis and the x axis was oriented normal to contact surface between the probe and prostate. The y axis was obtained by the right-hand rule.

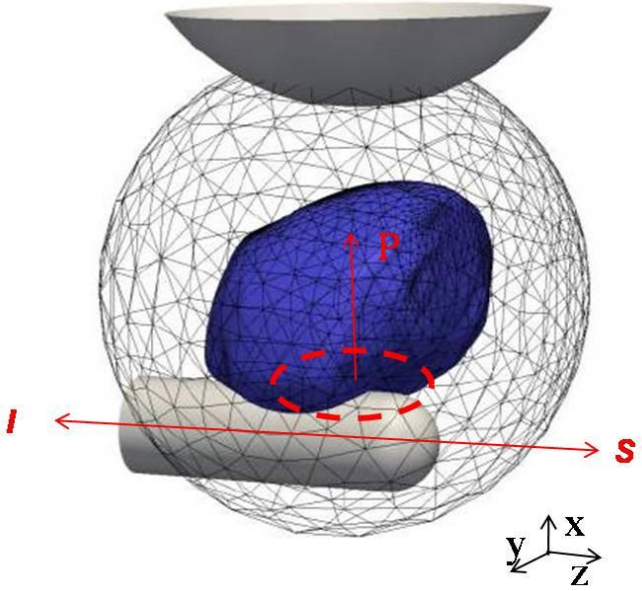

Fig. 5: Sample geometry of the prostate (solid surface in the middle) and the body object (wireframe sphere around the prostate). Force is applied on body mesh nodes that lie within the cylindrical shape of the endorectal probe. Position of the anterior side of the body object (at the top, intersection with the solid sphere part) is fixed. Image source: Lasso *et al.* [16]

2.7 Patient Data

Under ethics board approval, we have obtained five patient data sets from one of the clinical trials conducted with the device of Krieger *et al.* at the National Institutes of Health, USA. Each data set contained a target planning (reference) volume and a pre-needle insertion (tracking) volume used for biopsy position confirmation. The pre-needle insertion volume is motion-compromised since the prostate has moved relative to the previous target needle placement. A series of T2-weighted transverse slices (later reconstructed into a volume) were acquired by a spin echo sequence with a 1.5T GE Signa Excite MRI system. The reference volumes had resolutions of 0.78 x 0.78 x 4 mm/pixel for patient 1, 0.625 x 0.625 x 3 mm/pixel for patient 2, and 0.55 x 0.55 x 3 mm/pixel for patients 3, 4, and 5. The tracking volumes had resolutions of 0.78 x 0.78 x 4 mm/pixel for patient 1, 0.625 x 0.625 x 3 mm/pixel for patient 2, 0.85 x 0.85 x 3 mm/pixel for patients 3 and 4, and 0.94 x 0.94 x 3 mm/pixel for patient 5. The slice dimensions were 256 x 256 pixels for all patients. The acquired volumes varied from 16 to 25 transverse slices. We extracted three orthogonal slices from each pre-needle volume, centered in the prostate. As true sagittal and coronal slices were not available, they were obtained by interpolation between the transverse image slices.

3 Results

3.1 Simulation Tests

The ground truth displacements were created using the software-generated deformation field applied to the full pre-needle volume by the method described in section 2.6. We applied ± 5 degrees random rotation and ± 10 mm translation to the deformed volume along all axes and attempted to recover the introduced biopsy target displacement. Prior to performing the registration tests, we performed parameter tests (i.e. analyzed the effect of the three most influential parameters on the registration - MI sample size, B-spline grid resolution, and slice thickness, the results of which are shown in Fig. **6**,Fig. **7** and Fig. **8**, respectively. In each parameter test, the same reference/tracking volume pair was used (one of the 20 simulated volumes described in section 2.6) and all parameters were held constant except for the one being analyzed.

Voxel intensities were uniformly sampled from the prostate VOIs of the fixed and moving images. Sample populations were formed which were needed to calculate the joint probability density function for MI. The sample size was measured in percentage voxels of total VOI containing the prostate. Registration was tested for sample sizes ranging from 5% to 100%. Fig. 6 shows that TRE stays within a tight range of 1.50 to 2.50 mm and 0.50 to 1.00 mm for the rigid and deformable cases, respectively. Deformable TRE is lowest at 100% sampling (about 0.13 mm below that at 5%) but the change is negligible and the increase in registration time is significant. Thus, we set the sample size to 10% for the remainder of our registrations because increasing sample size further will increase registration time and render the algorithm unpractical.

Grid resolution is defined as the spacing between neighboring grid nodes in the x, y, and z directions, respectively. Grid resolution does not apply to rigid registration as the parameter is used only for defining the deformation grid in the image. Fig. 7 shows that improving grid resolution (i.e. reducing the spacing between grid nodes) beyond 40 × 40 × 20 mm did not improve deformable TRE. This is owed to the fact that the degrees of freedom of motion (i.e. number of unknown parameters of the cost function) increases which results in an increase in the odds of divergence from the solution. For the sake of curtailing both computational time and diverging risk, we chose 40 × 40 × 20

mm as the grid resolution for the remainder of our registrations.

The original slice thickness of the reference volume was 4 mm. For each slice thickness, the tracking volume was extracted from reference volume after being resampled in the through plane direction by slice averaging. We varied the tracking slice thickness over the typical range seen in interventional MRI scans reported in [14], which was 4-6 mm. The step size used was 0.5 mm. The result (Fig. 8) shows that TRE (rigid and deformable) decreases with increasing slice thickness up to 5 mm. This can be explained by the theory of direct proportionality between slice thickness and signal-to-noise ratio [23]. Increasing the thickness beyond 5 mm did not improve the TRE because there were too few slices in the reference volume to provide an accurate representation of the prostate. Since the original thickness of the dataset is already proximal to the average size of the tumor (4 mm), we chose to keep the slice thickness at the original value.

In order to assess whether three tracking slices are sufficient for estimating the out-of-plane deformation, registration tests were run on N_{slices} = 3, 4, and 5 slices. Due to superior resolution, transverse slices were added and positioned such that they bisected the prostate's superior and inferior halves. 20 registration tests were performed for each value of N, totaling the number of registrations to 60. The results are summed up in Table I. In Table I, TRE_{rigid} represents error of rigid registration alone while TRE_{def} represents the total error (rigid registration followed by deformable refinement) as defined by equation 1. The minimum, mean, and maximum values of the initial misalignment were 4.61, 10.10, and 14.58 mm, respectively.

TABLE I
SIMULATED RIGID AND DEFORMABLE REGISTRATION ERRORS FOR 3, 4, AND 5 TRACKING SLICES

N_{slices}	TRE_{rigid} (mm)	TRE_{def} (mm)	T_{rigid} (s)	T_{def} (s)
3	1.70	0.81	44	419
4	2.21	0.85	108	997
5	1.99	0.86	139	1731

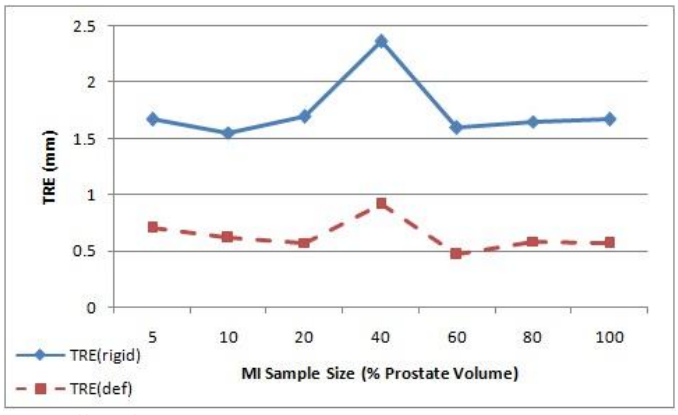

Fig. 6: Effect of MI sample size on registration error

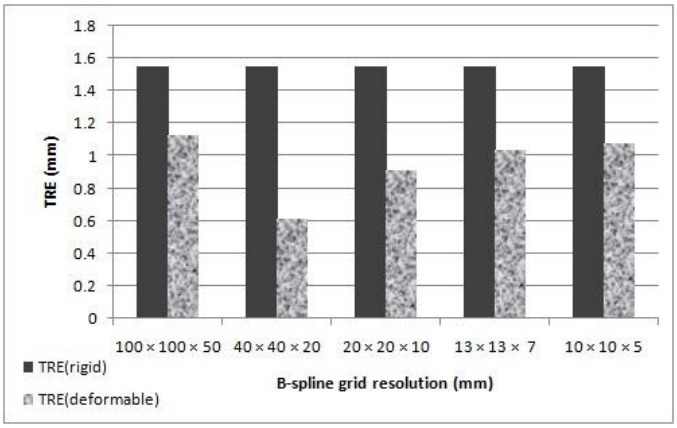

Fig. 7: Effect of B-spline grid resolution on registration error

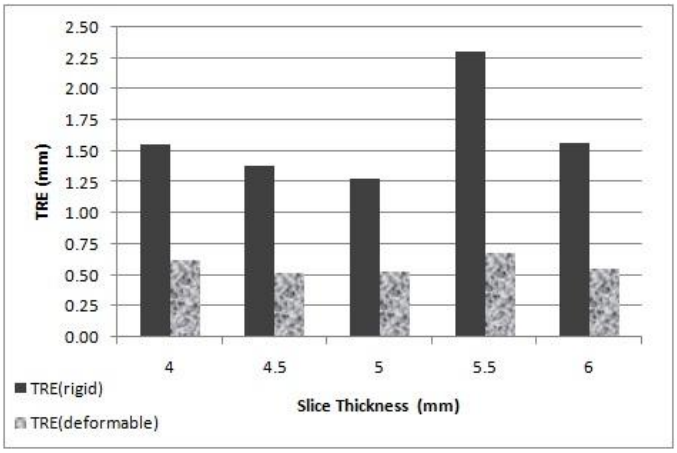

Fig. 8: Effect of Slice thickness on registration error

3.2 Patient Data Study

Our clinical study involved registration tests on five biopsy patients. These patients were chosen for registration tests for two reasons. First, their images had good contrast between the prostate and the surrounding tissues and had the least amount of distortions. Second, we selected patients with normal motion (less than 5.4 mm) and large motion (greater than 5.4 mm but less than 10mm) to analyze a broad but realistic spectrum of patient motions. Patient motion was measured in terms of target displacement (Fig. **9**) and was classified based on the average target displacement found by Xu *et al.* [3] (5.4 mm). Target displacement was defined as the distance between the pre-operatively planned position and motion-compromised intra-operative position of the biopsy target. As shown in Table II, D_T represents target displacement (mm), whose values were obtained from the findings of Xu *et al.* [3], as the patient data used were identical. As registration time was not of concern for needle placement validation, a full 3D-to-3D registration was performed (using all 20-25 slices) between pre-needle insertion and post-needle insertion volumes. However, for our purposes of real-time tracking, only three orthogonal slices (extracted) were used for registration.

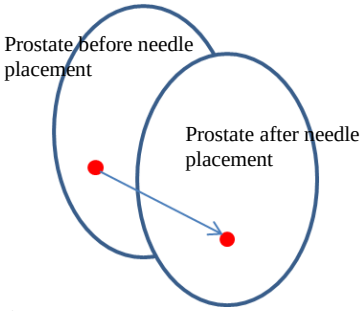

Fig. 9 Definition of target displacement by Xu *et al.* [3]

TABLE II
REGISTRATION RESULTS FOR PATIENT DATA (mm)

Patient No.	D_T	Rigid SDE	Deformable SDE
1	9.90	1.82	1.32
2	7.00	2.38	1.92
3	4.12	1.65	1.62
4	4.36	1.88	1.83
5	11.45	5.01	3.56
***Mean* ± SD**	**8.69 ±2.64**	**2.55 ± 1.40**	**2.05 ±0.87**

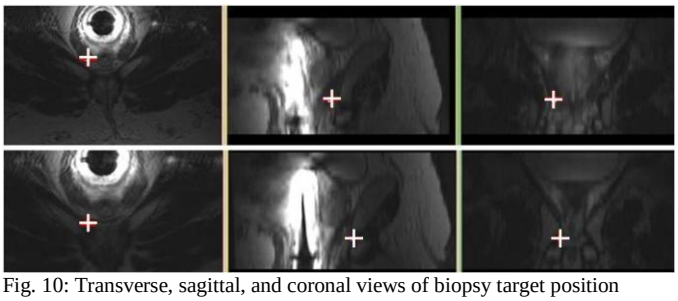

Fig. 10: Transverse, sagittal, and coronal views of biopsy target position before needle insertion (top) and after needle insertion (bottom)

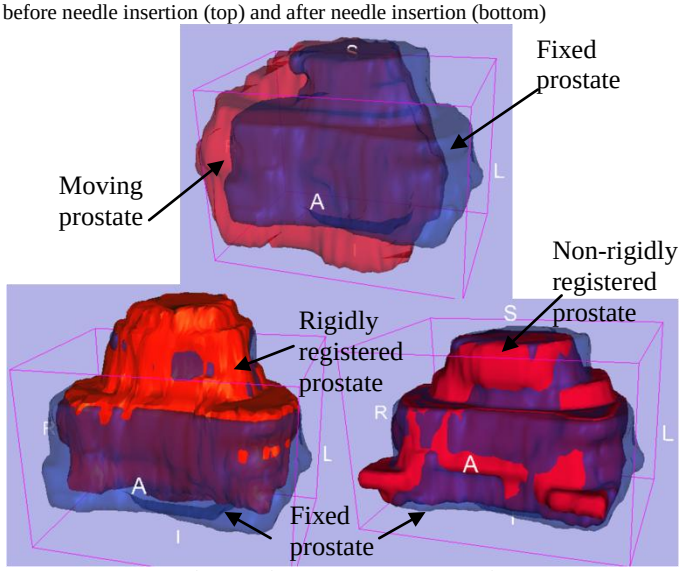

Fig. 11: Prostate surfaces before registration (top), after rigid registration (bottom left), and after deformable registration (bottom right). Just as in Table II, deformable registration shows no substantial benefits.

The average rigid registration time was 70s for the rigid algorithm and 1000s for the deformable algorithm (includes initial rigid alignment time). The originally planned (reference) position and the pre-needle insertion position of the first biopsy target for patient 1 are shown in Fig. **10**. The reference position was obtained from biopsy data and the pre-needle position was obtained by our tracking algorithm. The significance of Fig. **10** is that it shows where the target has moved since the time of reference volume acquisition.

The prostate surfaces before and after rigid and deformable registrations for patient 1 are shown in Fig. **11**. Note that the prostate was segmented for the purpose of validation. No segmentation was involved in the algorithm before or during registration.

4 Discussion

One major challenge for the evaluation of any registration method is the fact that in clinical patient data there is no ground truth. As such, registration accuracy cannot be evaluated in terms of the targets (TRE). Despite many computer-assisted interventions that use pre-operatively placed markers to perform registration or to evaluate TRE, no such landmarks are present in our data. Implanting markers for our study would involve discomfort and risk to the patient. Thus, the measure of registration error for actual patient registrations for this study was based on SDE as defined earlier in equation 2.

The relatively large variation of registration errors among the five patients is mainly due to the large time span over which the data were acquired and archived (5 years). During this time, devices (such as the endorectal coil integrated in the biopsy device) changed, which affected the imaging parameters such as SNR and resolution. As a result, experiments were performed on data that was already available and thus our results must be considered as preliminary.

Results of the simulated registration tests show that increasing the number of transverse tracking slices from 3 to 4 or 5 does not improve registration accuracy, implying that perhaps a significantly larger number of slices are required to improve registration accuracy. However, using more than 5 slices is time prohibitive. Nevertheless, registration results on the simulated data provided an insight into how the algorithm may behave in response to a typical patient motion in a clinical scenario.

The simulation study determined the accuracy and temporal performance trade-offs among three acquisition choices: 3, 4, or 5 transverse slices. Not only increasing the number of slices does not improve tracking accuracy, but the associated registration times increase. Rigid tracking using three slices offers fast results (44 s simulations, 70 s patient tests) and affordable error (1.70 mm simulations, 2.55 mm patient tests).

As observed from clinical registration results, the objective of 3 mm accuracy was achieved. It is important to note that this only accounts for the systematic error (i.e. registration error), not for external factors such as needle

deflection and segmentation. As long as the needle is placed within an accuracy of 4 mm (clinically significant size of a prostate tumor), the cancer is not likely to be missed. This gives the physician 1 mm room for needle deflection error. Since segmentation of the prostate surfaces was performed manually, segmentation error exists due to inter-user variability. The magnitude of this error is assumed to be negligible relative to the clinically significant size of tumor.

The acquisition time for one tracking slice is in the order of seconds and the positions of the tracking slices relative to the scanner's isocenter are set by the operator before the procedure. Acquisition time for tracking is negligible compared with computation time. The rigid registration times for both the simulation and patient tests seem proximal to clinical feasibility. Deformable registration times could raise feasibility concerns, but in all we are not particularly concerned about time, because for clinical trials the registration should be ported to the GPU which will obsolete concerns of temporal performance. The most computationally intensive parts of the algorithm (resampling and metric computation) can be parallelized and so we expect that a multi-threaded implementation on a multi-core CPU or GPU could reduce the execution time by a factor of 10.

In summary, our contribution was the development of rigid and non-rigid intensity based registration algorithms for tracking the biopsy targets in a robotic assisted MRI-guided prostate biopsy procedure. This algorithm should be adaptable in non-robotic procedures in other anatomical locations. Validation was performed on simulated patient MRI and clinical MRI. The rigid approach proved to be sufficient in the absence of GPU acceleration discussed earlier. Our algorithms have demonstrated convergent results for initial prostate displacements up to 14.6 mm (from simulations). Work continues with performing target registration error studies in typical sextant and octant biopsy locations and, most importantly, moving toward a prospective clinical trial with the use of true sagittal and coronal slices.

ACKNOWLEDGMENTS

The authors would like to thank the US national institutes of health (NIH) for providing data for the clinical trials. Hadi Tadayyon and Andras Lasso were partially supported by NIH R01 EB002963. Gabor Fichtinger was supported as Cancer Care Ontario Research Chair.

REFERENCES

[1] A. Jemal, R. Siegel, J. Xu, and E. Ward, "Cancer statistics, 2010," *CA: A Cancer Journal for Clinicians*, vol. 60, no. 4, pp. 277–300, 2010.

[2] A. Krieger, R. Susil, C. Menard, J. A. Coleman, G. Fichtinger, E. Atalar, and L. Whitcomb, "Design of a novel MRI compatible manipulator for image guided prostate interventions," *IEEE Transactions on Biomedical Engineering*, vol. 52, no. 2, 2005.

[3] H. Xu, A. Lasso, S. Vikal, P. Guion, A. Krieger, A. Kaushal, L. Whitcomb, and G. Fichtinger, "Accuracy validation for MRI-guided robotic prostate biopsy." SPIE, 2010.

[4] V. Karnik, A. Fenster, J. Bax *et al.*, "Assessment of image registration accuracy in three-dimensional transrectal ultrasound guided prostate biopsy," *Med Phys*, vol. 37(2), pp. 802–13, 2010.

[5] M. Baumann, P. Mozer, V. Daanen, and J. Troccaz, "Towards 3D ultrasound image based soft tissue tracking: a transrectal ultrasound prostate image alignment system." *MICCAI*, vol. 4792, pp. 26–33, 2007.

[6] C. Tempany, S. Straus, N. Hata, and S. Haker, "MR-guided prostate interventions," *JOURNAL OF MAGNETIC RESONANCE IMAGING*, vol. 27, pp. 356–367, 2008.

[7] I. Kaplan, N. Oldenburg, P. Meskella *et al.*, "Real time MRI-ultrasound image guided stereotactic prostate biopsy," *Magnetic Resonance Imaging*, vol. 20, pp. 295–299, 2002.

[8] S. Xu, J. Kruecker, P. Guion, N. Glossop, Z. Neeman, P. Choyke, A. K. Singh, and B. J. Wood, "Closed-loop control in fused MR-TRUS image-guided prostate biopsy," *MICCAI*, vol. 10(1), pp. 128–135, 2007.

[9] J. Chappelow, B. N. Bloch, N. Rofsky, E. Genega, R. Lenkinski, W. DeWolf, and A. Madabhushi, "Elastic registration of multimodal prostate MRI and histology via multiattribute combined mutual information," *Medical Physics*, vol. 38, no. 4, pp. 2005–2018, 2011. [Online]. Available: http://link.aip.org/link/?MPH/38/2005/1

[10] N. Hata, M. Jinzaki, D. Kacher *et al.*, "MR imaging - guided prostate biopsy with surgical navigation software: Device validation and feasibility," *Radiology*, vol. 220, pp. 263–268, 2001.

[11] N. Hata, J. Tokuda, S. Morikawa, and T. Dohi, "Projection profile matching for intraoperative MRI registration embedded in MR imaging sequence," *MICCAI*, pp. 164–169, 2002.

[12] A. Bharatha, M. Hirose, N. Hata, S. K. Warfield, M. Ferrant, K. H. Zou, E. Suarez-santana, J. Ruiz-Alzola, A. D'Amico, R. A. Cormack, R. Kikinis, F. A. Jolesz, and C. M. C. Tempany, "Evaluation of three-dimensional finite element-based deformable registration of pre- and intra-operative prostate imaging," *Med. Phys.*, vol. 28 (12), pp. 2551–60, 2001.

[13] S. Oguro, J. Tokuda, H. Elhawary *et al.*, "MRI signal intensity based b-spline nonrigid registration for preand intraoperative imaging during prostate brachytherapy," *J Magn Reson Imaging.*, vol. 30(5), pp. 1052–1058, 2009.

[14] B. Fei, J. L. Duerk, D. T. Boll, J. S. Lewin, and D. L. Wilson, "Slice-to-volume registration and its potential application to interventional MRI-guided radio-frequency thermal ablation of prostate cancer," *IEEE Transactions on Medical Imaging*, vol. 22, no. 4, 2003.

[15] S. Gill, P. Abolmaesumi, and S. Vikal, "Intraoperative prostate tracking with slice-to-volume registration in MR," *International Conference of the Society for Medical Innovation and Technology*, pp. 154–158, 2008.

[16] [16] H. Tadayyon, A. Lasso, S. Gill, A. Kaushal, P. Guion, and G. Fichtinger, "Target motion compensation in MRI-guided prostate biopsy with static images." 32nd Annual International IEEE EMBS Conference, 2010.

[17] H. Singh, E. I. Canto, and S. F. e. a. Shariat, "Improved detection of clinically significant, curable prostate cancer with systematic 12-core biopsy," *J Urol*, vol. 171, p. 1089, 2003.

[18] B. Fei, C. Kemper, and D. L. Wilson, "Three-dimensional warping registration of the pelvis and prostate," vol. 4684. SPIE, 2002.

[19] M. Zhang, R. Alhajj, and J. Rokne, "Effectiveness of optimal incremental multi-step nearest neighbor search," *Expert Systems with Applications*, vol. 37, no. 8, pp. 6018 – 6027, 2010.

[20] N. Hansen, "The CMA evolution strategy: A comparing," *Springer*, pp. 75–102, 2006.

[21] A. Lasso, S. Avni, and G. Fichtinger, "Targeting error simulator for image-guided prostate needle placement." 32nd Annual International IEEE EMBS Conference, 2010.

[22] J. Hensel, C. Menard, P. Chung *et al.*, "Development of multiorgan finite element-based prostate deformation model enabling registration of endorectal coil magnetic resonance imaging for radiotherapy planning," *International Journal of Radiation Oncology * Biology * Physics*, vol. 68, pp. 1522–1528, 2007.

[23] D. Nishimura, "Principles of magnetic resonance imaging," p. 163, 2010.